JOURNAL OF SOLID STATE CHEMISTRY 120, 299–310 (1995)

$Cs(TiAs)O_5$ and $Cs(TiP)O_5$: A Disordered Parent Structure of $ABOCO_4$ Compounds

M. Kunz,*,[1] R. Dinnebier,† L. K. Cheng,‡ E. M. McCarron,‡ D. E. Cox,§ J. B. Parise,* M. Gehrke,‡ J. Calabrese,‡ P. W. Stephens,† T. Vogt,§ and R. Papoular§

*CHiPR and Department of Earth and Space Sciences, SUNY, Stony Brook, New York; †Department of Physics, SUNY, Stony Brook, New York; ‡E.I. duPont Nemours & Co., Experimental Station, Wilmington, Delaware; and §Department of Physics, Brookhaven National Laboratory, Upton, New York

Received March 23, 1995; in revised form July 19, 1995; accepted July 26, 1995

The structures of the two isostructural compounds Cs(TiAs)O_5 (CTA) and Cs(TiP)O_5 (CTP) were solved and refined by application of the Rietveld profile technique to high-resolution synchrotron X-ray and neutron powder data. The structures are cubic, space group $Fd\bar{3}m$ with a = 10.23415(5) Å (CTA) and a = 10.08733(2) Å (CTP), and are characterized by an unusual framework consisting of randomly disordered TiO_6 octahedra and XO_4 (X = As, P) tetrahedra with the Cs^+ cation occupying large cavities within this framework. The lack of long-range order between octahedra and tetrahedra simulates partially occupied octahedra shared by Ti and X with large displacement parameters for both cations and oxygens. The Ti,X-site can be resolved as a split-atom position where the tetrahedral metal is shifted from the center toward the edge formed by the octahedral oxygens. Split-oxygen positions were refined from a combination of X-ray and neutron data for CTA. The cubic structure is related to the orthorhombic $KTiOPO_4$-type structure in that the latter can be derived from the former by ordering of the TiO_6 octahedra and PO_4 tetrahedra. Since different ordering schemes applied to the cubic CTA/CTP structure lead to other known ordered structures of the same stoichiometry such as $K(Mg_{1/3}Nb_{2/3})OPO_4$ and γ-$NaTiOPO_4$, cubic CTA/CTP can be viewed as the "mother of all $ABOCO_4$-structures." The elucidation of the cubic structure allows us to propose a quantified "threatened structure model," which helps in the understanding of the mechanism of this phase transition. © 1995 Academic Press, Inc.

INTRODUCTION

$CsTiOAsO_4$ (CTA) crystallizes at room temperature in space group $Pna2_1$ (1) and is isostructural with the well-known nonlinear optical compound $KTiOPO_4$ (KTP) (2). Like KTP, it also exhibits strong nonlinear optical behavior and its low absorption in the midinfrared range makes it a desirable material for both frequency sum generation and optical parametric oscillation in this frequency range (3).

Cheng *et al.* (3, 4) found CTA to undergo a phase transition to a cubic phase at 963°C, which could be retained at room temperature either by heating the orthorhombic phase to 970°C and subsequently quenching, or by flux-growth. The X-ray powder pattern of this cubic phase is similar to the one reported in (5) for $CsTiPO_5$ (CTP) and an analogous cubic phase is also observed for $RbTiOPO_4$ (RTP) and $TlTiOPO_4$ (TTP) (2). The first-order nature of the phase transition as well as the powder pattern of the cubic phase are clearly different from the ferroelectric high-temperature phase transition observed for KTP at its Curie temperature (6).

In order to fully explore the possible technological applications of the strongly nonlinear optical properties of orthorhombic CTA, it is essential to grow large single crystals of high quality. This goal, however, is hampered by the phase transition from the cubic phase at 963°C, which leads to extended twinning and domain growth. Determination of the cubic structure is a necessary step toward the understanding of this phase transition and the design of alternative synthesis routes which avoid the transition. In this paper, we report the crystal structures of cubic Cs(TiAs)O_5 and Cs(TiP)O_5, which were solved and refined using high-resolution synchrotron X-ray and neutron-powder diffraction data in combination with the Rietveld profile technique.

EXPERIMENTAL PROCEDURE

Small crystals of cubic $CsTiXO_5$, with X = (P or As), were grown by the spontaneously nucleated slow-cooling technique using a $CsXO_3$ flux. Reagent grade materials were used in all preparations. Colorless crystals of cubic Cs(TiAs)O_5 (ca. 0.5—1 mm^3) were obtained by cooling a solution of 41 mole% Cs_2O, 19 mole% TiO_2, and 40 mole% As_2O_5 from 1000 to 750°C. For cubic Cs(TiP)O_5, the As_2O_5

[1] Present address: High Pressure Group, ESRF, BP-220, Av. des Martyrs, F-38043 Grenoble Cedex, France.

0022-4596/95 $12.00

TABLE 1
Chemical Composition of $Cs(TiAs)O_5$ and $Cs(TiP)O_5$

Oxides	$Cs(TiAs)O_5$ (wt%)	$Cs(TiP)O_5$ (wt%)
Cs_2O	41.7(12)	47.7(14)
TiO_2	24.6(9)	29.2(9)
X_2O_5	35.4(12)	23.2(4)
Total	101.7	100.1
	Elements	
	Normalized atom-fraction (based on 5 oxygens)	Normalized atom-fraction (based on 5 oxygens)
Cs	0.96(5)	0.99(4)
Ti	1.00(1)	1.06(2)
X (X = As, P)	1.00(1)	0.95(1)
Sum of cations	2.96(7)	3.00(7)

in the above solution was replaced with P_2O_5, and the melt cooled from 1050 to 800°C. Unlike $Cs(TiAs)O_5$, only microcrystals (<50 μm) of $Cs(TiP)O_5$ were obtained.

Chemical analyses of the two compounds were made with a Camebax electron microprobe in wavelength dispersive mode operating at 10 kV accelerating voltage and 10 nA beam current. CsI, apatite ($Ca_5(PO_4)_3(OH, F)$), rutile (TiO_2), and InAs were used as standards, and the data corrected using the $\phi(\rho Z)$-procedure of (7). Table 1 gives the average of 18 (CTA) and 10 (CTP) determinations on different grains.

Preliminary experiments with an optical microscope confirmed the cubic crystal system for CTA and CTP by their isotropic optical behavior under crossed polarizers. Long-term precession photographs as well as TEM diffraction pictures showed satellite reflections at $(h, k, l)n/3$ (n = 0, 1, 2), Fig. 1, which can be explained by either a triple supercell or (multiple) twinning through {111} as the twin plane (Spinel-law) (8). Spinel twin-domains are related to each other by a mirror operation through {111} planes, which generates additional reflections at $(h, k, l)n/3$ (n = 1, 2). If these satellite reflections are ignored, there are two possible space groups, $Fd\bar{3}$ or $Fd\bar{3}m$, determined from precession photographs on the basis of systematic absences. Attempts to solve an average structure of a hypothetical triple-superstructure with single-crystal X-ray diffraction data failed. Single-crystal data sets showed high disagreement between symmetry equivalent reflections, indicating that the reflections were affected by twinning. In order to solve the structure of these strongly twinned materials, high resolution powder data were collected at beamlines X3B1 (CTA) and X7A (CTP) at the Brookhaven National Synchrotron Light Source (NSLS). In addition, a dataset from CTA was collected at the high-resolution neutron powder diffractometer (HRNPD) at beamline

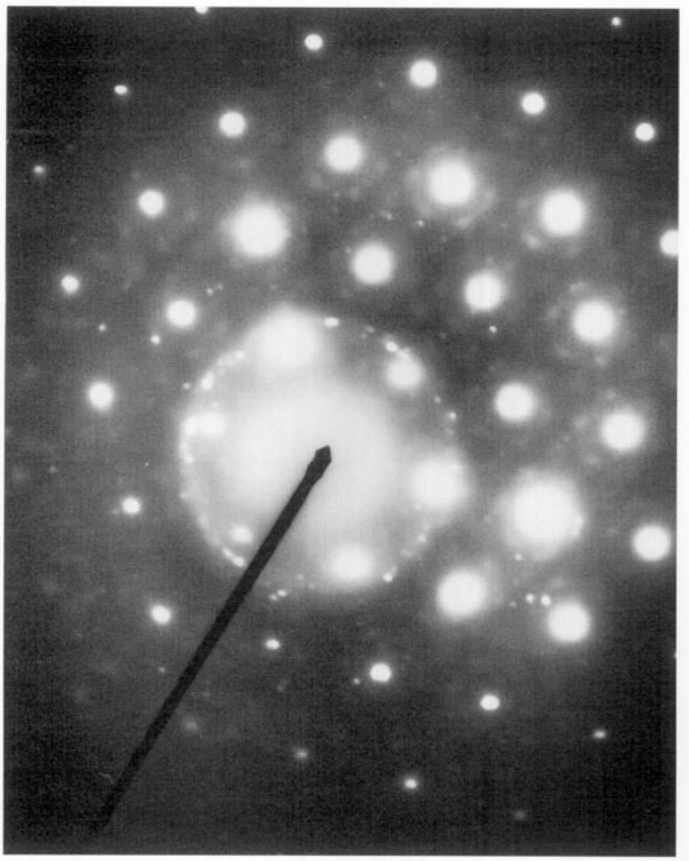

FIG. 1. TEM diffraction picture of CTA along [111]. Note the satellite reflections at $(h, k, l)n/3$ (n = 1, 2) indicative of multiple twinning along the {111} plane (Spinel-law).

H1A at the Brookhaven High Flux Beam Reactor (HFBR). The absence of any satellite reflections in all of these powder diffraction experiments confirms the assumption that the satellites observed during single-crystal diffraction are caused by twinning.

For the X-ray experiment on CTA, a wavelength of 0.6993(2) Å was selected from a double-crystal Si(111) monochromator. A NaI scintillation detector was used to record the diffracted beam from a flat plate sample. The resolution was additionally increased by placing a Ge(111) crystal with neglectable mosaic spread in front of the detector. Data were collected over an angular range of 2Θ between 10.0° and 50.0° at step intervals of 0.005° and a counting time of 2 sec for each step, yielding a total of 63 reflections. A θ-scan revealed significant intensity variations. This is caused by a θ-dependent variation of grain volume under diffraction conditions due to irregular grain size distribution even after extensive grinding. The sample was therefore rocked over 5° to minimize this effect. The peak FWHM ranged between 0.015° and 0.051° 2Θ. The apparently high increase of FWHM with 2Θ is caused by the high resolution excluding most of the instrumental

broadening at low angles and therefore revealing the whole range of sample broadening at high angles.

The neutron data were collected at a wavelength of 1.886(2) Å. The monochromator consisted of a 30-cm vertical and 5-cm horizontal array of 24 Ge(511) crystals at a take-off angle of 120°, providing a beam cross section of 4.5×2.5 cm^2. Five-foot collimators were used before the monochromator and in the detector bank, which consists of 64 ^{3}He counters covering a range of 160°. A detailed description of the diffractometer and the monochromator has been given elsewhere (9–11). A free-standing pellet, 1 cm in diameter and 2 cm in length was placed at the sample position and a scan was carried out at 0.02° steps with a counting time of roughly 5 min per step. The data were corrected for both detector efficiency and positional error and yielded 40 reflections between 10° and 155° 2Θ. The peak FWHM ranged between 0.21° and 0.44° 2Θ.

X-ray data from CTP were collected at a wavelength of 0.7005(2) Å selected from a channelcut Ge(111) monochromator with a linear position-sensitive multiwire detector operating in the escape mode under a krypton gas pressure of 43 psi. The detector was moved in steps of 0.25° 2Θ, yielding a pattern containing 102 reflections over an angular range between 5.5° and 60.0° 2Θ. The peak FWHM ranged between 0.036° and 0.07° 2Θ.

STRUCTURE SOLUTION AND REFINEMENT

For all three datasets, the observed spectra were first fitted using LeBail's method of intensity extraction (12) while varying peak-profile parameters, lattice constants, and a 2Θ zero-offset correction. Background was interpolated between selected points well-removed from peaks. Peak-profile functions were modeled using a multiterm Simpson's rule integration (13) of the pseudo-Voigt function described by (14) as implemented in GSAS (15). The peak asymmetry at low angles in the CTA X-ray dataset was very pronounced due to the 5° rocking angle. Since these peak shapes could not be modeled with the available profile functions, the low-angle section of the CTA X-ray dataset was excluded below 15° 2Θ. After convergence of the LeBail fit, the peak profile parameters and zero-point corrections were fixed before proceeding with the structure refinement. Further refinement details are given in Table 2.

The structure was solved in space group $Fd\bar{3}m$ (Nr. 227) from the CTA X-ray data by direct methods using the program package SIRPOW (16). The solution initially yielded one Cs position in 8*b*, one oxygen position in 48*f*, and an apparently octahedrally coordinated second metal positioned in 16*c* sites. The latter showed an electron density corresponding to 0.5 Ti + 0.5 *X* (*X* = As, P). Since difference Fourier maps did not show any significant residual peaks, a random mixture of Ti and *X* was assigned to the 16*c* position. This model was subsequently refined with the Rietveld technique using the program package GSAS (15).

TABLE 2
Rietveld Refinement Details for $Cs(TiAs)O_5$ and $Cs(TiP)O_5$

	$Cs(TiAs)O_5$ (neutrons)[a]	$Cs(TiAs)O_5$ (X-ray)[a]	$Cs(TiP)O_5$ (X-ray)[b]
Refinement software	GSAS	GSAS	GSAS
Number of intensities extracted	45	69	98
Spacegroup	$Fd\bar{3}m$(227)	$Fd\bar{3}m$(227)	$Fd\bar{3}m$(227)
Wavelength (Å)	1.886(2)	0.6993(1)	0.7005(2)
$\vec{a}$ (Å)	10.23415(5)	10.23415(1)	10.08733(2)
R_p (%)	5.06	6.63	3.65
R_{wp} (%)	7.41	9.72	5.80
$R(F^2)$	11.18	12.98	13.22
$R(F)$	7.91	10.62	9.48

[a] Oxygen atoms split.
[b] Average oxygens.

All structure refinements were carried out with scattering factors for neutral atoms. The scattering densities in the (TiAs) and (TiP) positions were initially refined, yielding values of 27.8(2) and 18.8(2) electrons, respectively. The occupancy of this position was therefore fixed at 0.5 Ti and 0.5 As for CTA and 0.53 Ti and 0.47 P for CTP, in accordance with the microprobe results, Table 1. The oxygen occupancy refined to a value of 0.827(5) and was therefore fixed at 5/6 in the initial refinements, this value also being in accordance with the stoichiometry obtained from microprobe data, Table 1. Refinements based on this disordered model gave average coordinate values for the metal and oxygen positions, not surprisingly with large displacement parameters.

It is obvious that a model in which Ti and *X* occupy

TABLE 3
Coordinates and Displacement Parameters U_{ij} (Å^2 × 100) for $Cs(TiAs)O_5$ and $Cs(TiP)O_5$

Atom	*x*	*y*	*z*	U_{iso}	Occupancy
		$Cs(TiAs)O_5$ (neutron and X-ray combined)			
Cs	$\frac{3}{8}$	$\frac{3}{8}$	$\frac{3}{8}$	4.31(8)	1.0
Ti	0.0	0.0	0.0	2.9(2)	$\frac{1}{2}$
As	−0.0402(5)	0.0	0.0402(5)	2.9(2)	$\frac{1}{2}$
O(1*a*)	−0.0604(6)	$\frac{1}{8}$	$\frac{1}{8}$	3.29(9)	$\frac{5}{12}$
O(1*b*)	−0.0696(7)	0.0872(7)	0.1400(7)	3.29(9)	$\frac{1}{12}$
O(2)	−0.100(1)	0.0256(9)	−0.0169(7)	3.29(9)	$\frac{1}{24}$
		$Cs(TiP)O_5$ (X-ray)			
Cs	$\frac{3}{8}$	$\frac{3}{8}$	$\frac{3}{8}$	2.53(2)	1.0
Ti	0.0	0.0	0.0	1.9(1)	0.53
P	−0.0389(7)	0.0	0.0389(7)	1.9(1)	0.47
O(1)	−0.0585(2)	$\frac{1}{8}$	$\frac{1}{8}$	6.5(1)	$\frac{5}{6}$

TABLE 4
Selected Bond Lengths for Cubic $Cs(TiAs)O_5$ and $Cs(TiP)O_5$

	$Cs(TiAs)O_5$	$Cs(TiP)O_5$
Cs–O(6*x*)	3.192(3)	3.184(5)
Cs–O(12*x*)	3.673(2)	3.627(5)
Ti–O(1*a*)	1.921(4)	1.881(1)
Ti–O(1*b*)	1.832(7)	Not refined
Ti–O(1*b*)	2.133(7)	Not refined
As–O(1*b*)	1.541(7)	Not refined
As–O(1*b*)	1.711(8)	Not refined
As–O(1*b*)	1.803(9)	Not refined
As–O(2)	1.592(9)	Not refined

Note. All values except the As–O bonds are derived from the disordered model refined with X-ray data.

an octahedron represents an average not only over two different metal sites but also over two different coordination polyhedra, since Ti is expected to be octahedrally coordinated and *X* is presumably in tetrahedral coordination. To characterize these different coordination polyhedra, an attempt was made to refine the metal and oxygen sites as split-atom positions. Starting models were obtained by geometric reasoning and by maximum entropy methods, based on the assumption that the octahedra and tetrahedra, although randomly distributed, have to be mutually connected in order to maintain a coherent framework. This implies that at least two oxygens of each coordination polyhedron have to be coordinated to both, Ti and *X*, and the models were assumed to have split Ti, *X* positions as well as two oxygen positions. O(1) was assumed to be common to both the Ti and *X* coordination polyhedra, with O(2) completing the tetrahedron. The expected occupancies are therefore such that, out of the 40 oxygens per

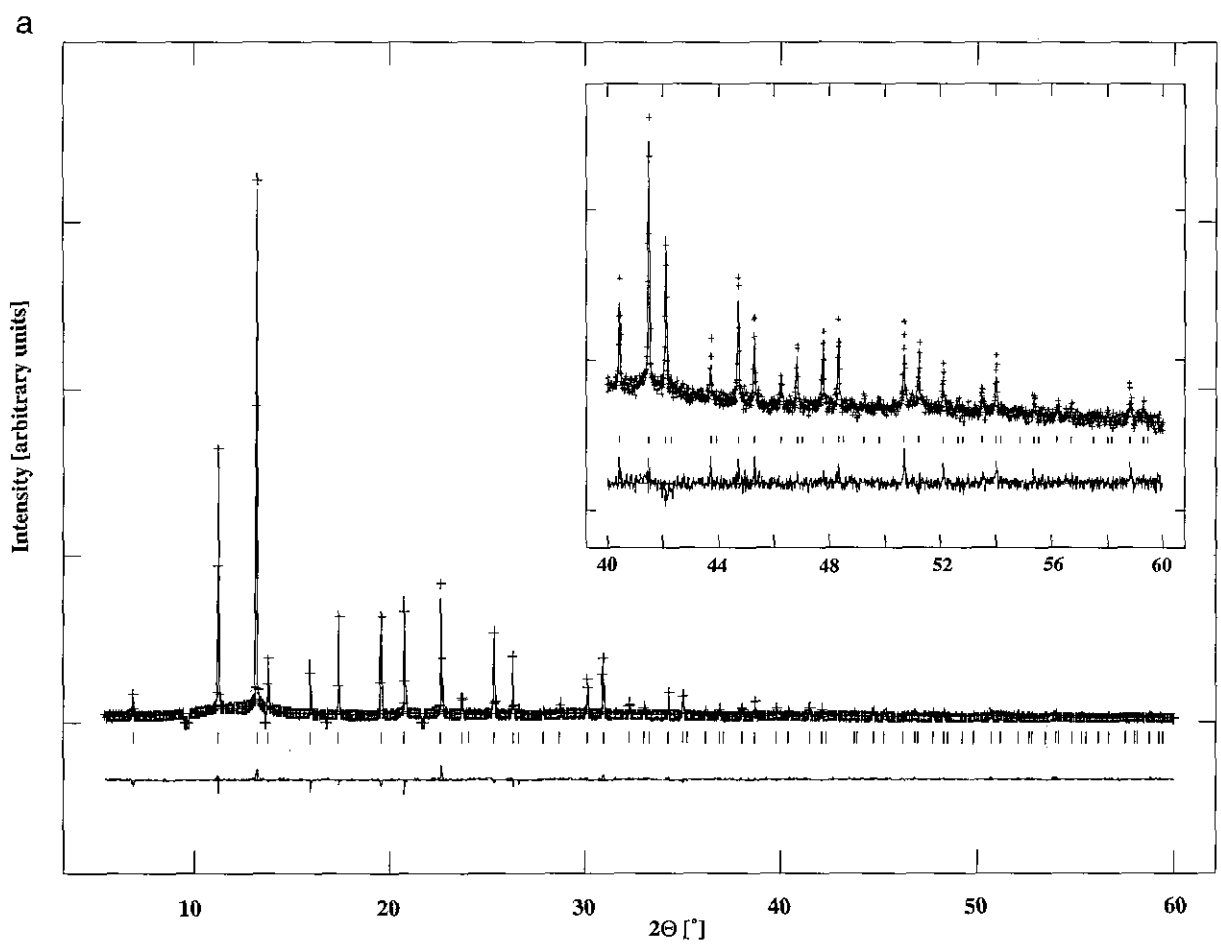

FIG. 2. Powder diffraction pattern of (a) cubic CTP (X-rays), (b) cubic CTA (X-rays) and (c) cubic CTA (neutrons). Observed pattern, plus marks; calculated pattern, solid line; difference curve given below. Note that due to the high resolution of the pattern and the limited resolution of the printer, not all observed points are plotted.

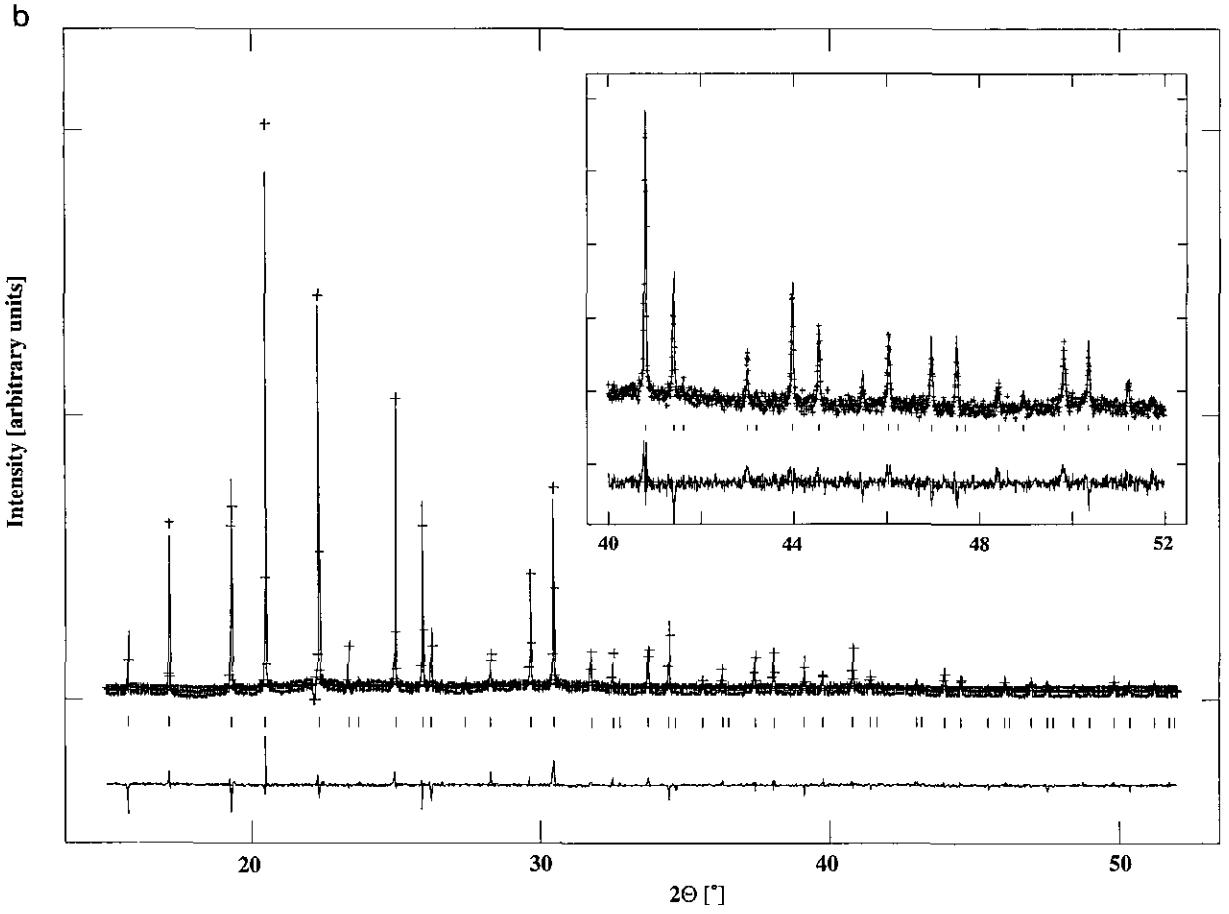

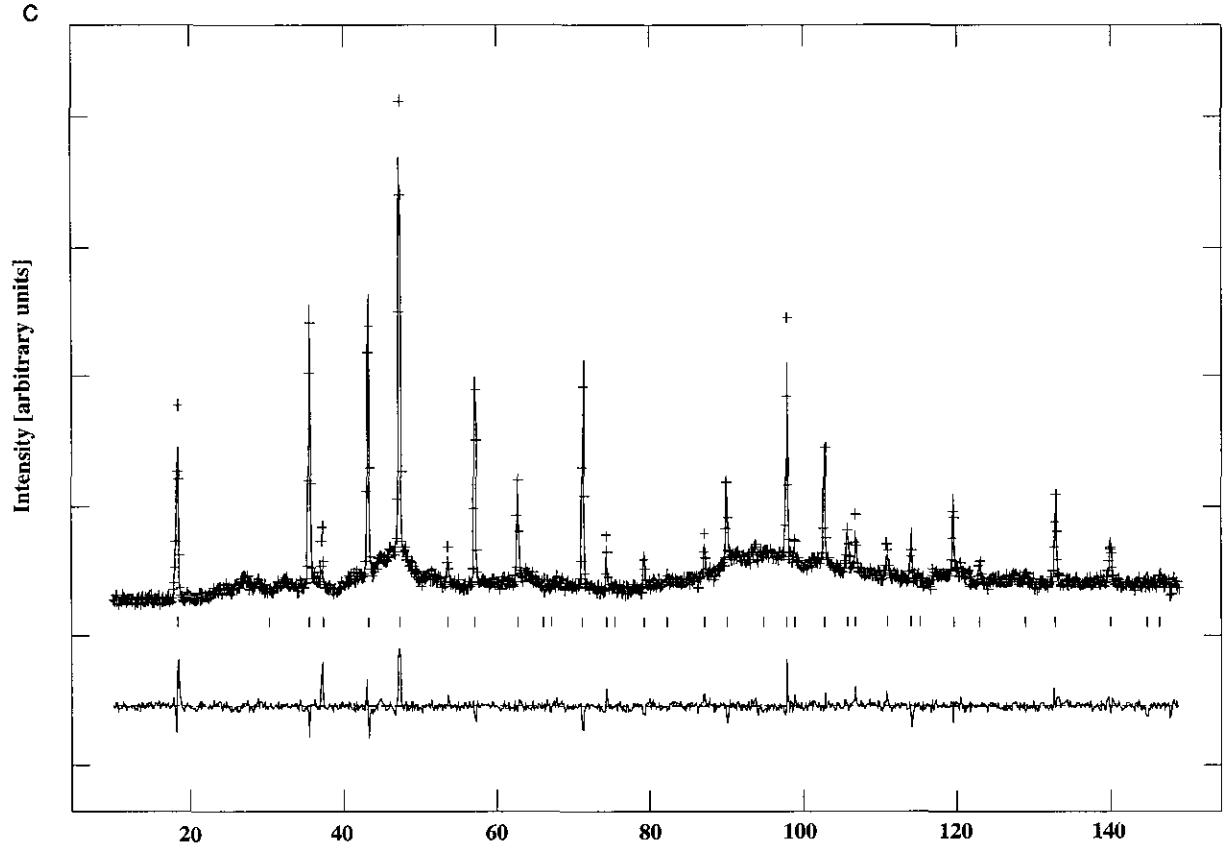

FIG. 2—*Continued*

unit cell, 32 are O(1) and only 8 are O(2). The isotropic temperature factors for Ti and X were constrained to be equal as were those of O(1) and O(2).

For CTP, attempts to refine various split-atom models were hampered by convergence problems, for example, while the off-center tetrahedral cation refined readily into a stable positon toward one edge of the O(1)-octahedron, the tetrahedra oxygen O(2) position remained ill-defined and oscillated wildly. Possible O(2) positions extracted during the refinements all yielded unreasonable crystal-chemical geometries, and we therefore abandoned a split-oxygen model for CTP in favor of an average model with a split-metal site. The failure to refine a plausible split-oxygen position can be explained by the low occupancy of these sites due to the strong disorder.

Attempts to refine a split model for CTA using both the neutron and X-ray data pointed clearly toward a split model. A refinement based on 2 oxygen positions converged to a neutron-$R(F^2)$ of 11% compared to 30% for a disordered model with only 1 oxygen. However, the isotropic displacement parameter U_{iso} of the oxygens remained large (0.06 Å^2) and the refined positions did not form an acceptable coordination sphere around As. A refinement based on 3 oxygens was therefore carried out with the O1 position split into two sites. Although this did not produce a significant improvement in $R(F^2)$, the refined oxygen positons were consistent with both TiO_6 octahedra and AsO_4 tetrahedra. In addition, U_{iso} for the oxygens refined to reasonable values of about 0.035 Å^2. For CTA, a split-atom model with 3 oxygens was therefore favored over a disordered model with only one oxygen position.

RESULTS

Refined coordinates and displacement parameters are given in Table 3 and selected bondlengths are listed in Table 4. Fig. 2 shows the Rietveld profile fits and difference plots for the two structures.

The structure is characterized by a corner-linked framework consisting of a disordered array of TiO_6 octahedra and XO_4 tetrahedra. The Cs^+ cations are located in large cavities within the framework, each Cs being coordinated on average to 5 + 10 oxygens. Over the coherence length of the X-ray experiment, the long-range disorder of tetrahedra and octahedra over a set of equivalent positions simulates a single octahedron occupied by either Ti^{4+} or X^{5+} with a partially occupied oxygen position forming the octahedral corners. The different local coordination around Ti^{4+} and X^{5+} is, however, already strongly suggested in the average model by a splitting of the Ti^{4+} and X^{5+} position, where the tetrahedral metal partially occupies symmetrically equivalent positions displaced from the octahedral center towards the edges.

In the split model refined for CTA from the combined neutron and X-ray data sets, two additional oxygen positions were resolved, consistent with a tetrahedral oxygen arrangement around the As-atom. The tetrahedra are formed by 3 O1b and one O2 atoms, whereas the regular TiO_6 octahedra are formed from 6 O1a oxygens. If locally a TiO_6 octahedron is connected to an AsO_4 tetrahedron, however, the bridging oxygen is O1b rather than O1a, leading to a slightly distorted TiO_6 octahedron similar to those observed in the orthorhombic phase, Table 4. However, it was not possible to bootstrap the split-atom CTA model with the CTP X-ray dataset. This is not too surprising, since a combination of neutron and X-ray data sets was needed to resolve the O-splitting in CTA. It is important to note that this should not be interpreted as an indication of 6-coordinated phosphorous in cubic CTP, but rather that the disorder in CTP is such that it is not possible to unambiguously resolve split-oxygen positions in the presence of heavy scatterers like Cs with an X-ray data set only. The collection of a neutron data set with CTP has not been possible so far due to the small amount of sample available. Further investigations using NMR are under way in order to explore the local tetrahedral coordination of P^{5+} in CTP.

In the final stages of refinement, various models were tried with Cs and Ti placed on lower symmetry sites in order to investigate possible split-atom positions caused by the high degree of disorder in this structure. Only a few attempts did not diverge, and these showed only a slight improvement in all agreement factors and were rejected on the basis of a Hamilton significance test applied to $R(F^2)$ (17).

The very pronounced and irregular background in the neutron data set can be explained by short-range correlations within the disordered structure which show up in the neutron pattern as broad bumps in the background. This is confirmed by a radial distribution calculation (GSAS) carried out on the neutron background revealing strong peaks at distances corresponding to observed O–O (2.87 Å) and metal–metal distances (4.2 Å, 5.1 Å).

DISCUSSION

The disordered CTA/CTP structure can be described as consisting of "octahedral" layers parallel {111} equivalent to those in hexagonal tungsten bronze (HTB) layers (18, 19), Fig. 3, ("octahedral" here meaning the disordered array of octahedra and tetrahedra as described above). These layers are stacked along ⟨111⟩ directions. While in HTB the individual layers are stacked directly on top of each other and are symmetrically related via a mirror plane (ABABAB...); neighboring HTB-type layers in cubic CTA/CTP are separated by an additional layer consisting

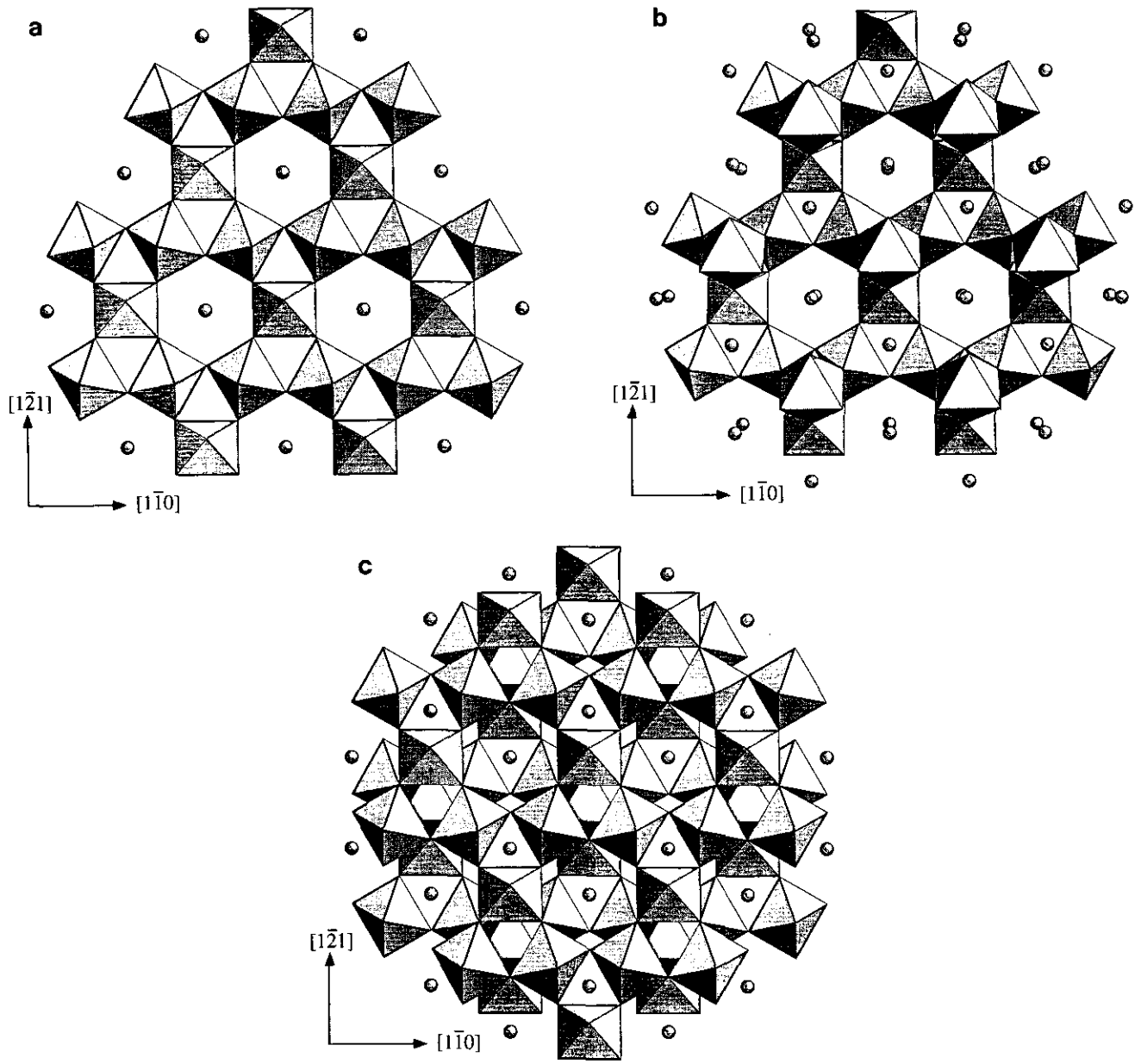

FIG. 3. (a) HTP-type layer of cubic CTA/CTP cut parallel {111}. (b) Layer of isolated octahedra on top of HTB-layer. (c) Two HTB-type layers separated by isolated octahedra. Note the shift of $(\frac{1}{3})$ [1 $\bar{2}$ 1] between alternating HTB-type layers.

of isolated "octahedra" placed on top of the centers of the characteristic HTB-type "octahedral" triangles, Fig. 3b. Each two equivalent (HTB-type or isolated octahedra) layers are shifted by (1/3)[1$\bar{2}$1] relative to each other, causing an ($A_1B_1A_2B_2A_3B_3A_1B_1$..)-type stacking, Fig. 3.

The disordered structure of cubic CTA and CTP has a very straightforward relationship to that of the orthorhombic *Pna*2_1-phase and can be transformed into the latter by ordering of the octahedra and tetrahedra, Fig. 4. The transformation matrix between the two cells is $a_{orth} \rightarrow [110]_{cub}$; $2 \cdot b_{orth} \rightarrow [\bar{1}10]_{cub}$; $c_{orth} \rightarrow c_{cub}$. The characteristic octahedral chains of the orthorhombic phase are found in the cubic structure as chains of mixed polyhedra. In the disordered model, where these polyhedra are depicted as octahedra, these chains appear almost identical to the ordered chains in the orthorhombic phase, Fig. 4.

A similar relationship can also be found between the CTP/CTA structure and the tetragonal structure of $K(Mg_{1/3}Nb_{2/3})PO_5$ (KMNP) (20), where a different ordering scheme imposed on the cubic CTA/CTP structure leads to a tetragonal structure with corner-linked *cis–cis* Ti chains arranged in a screw-like fashion around a 4_1 screw

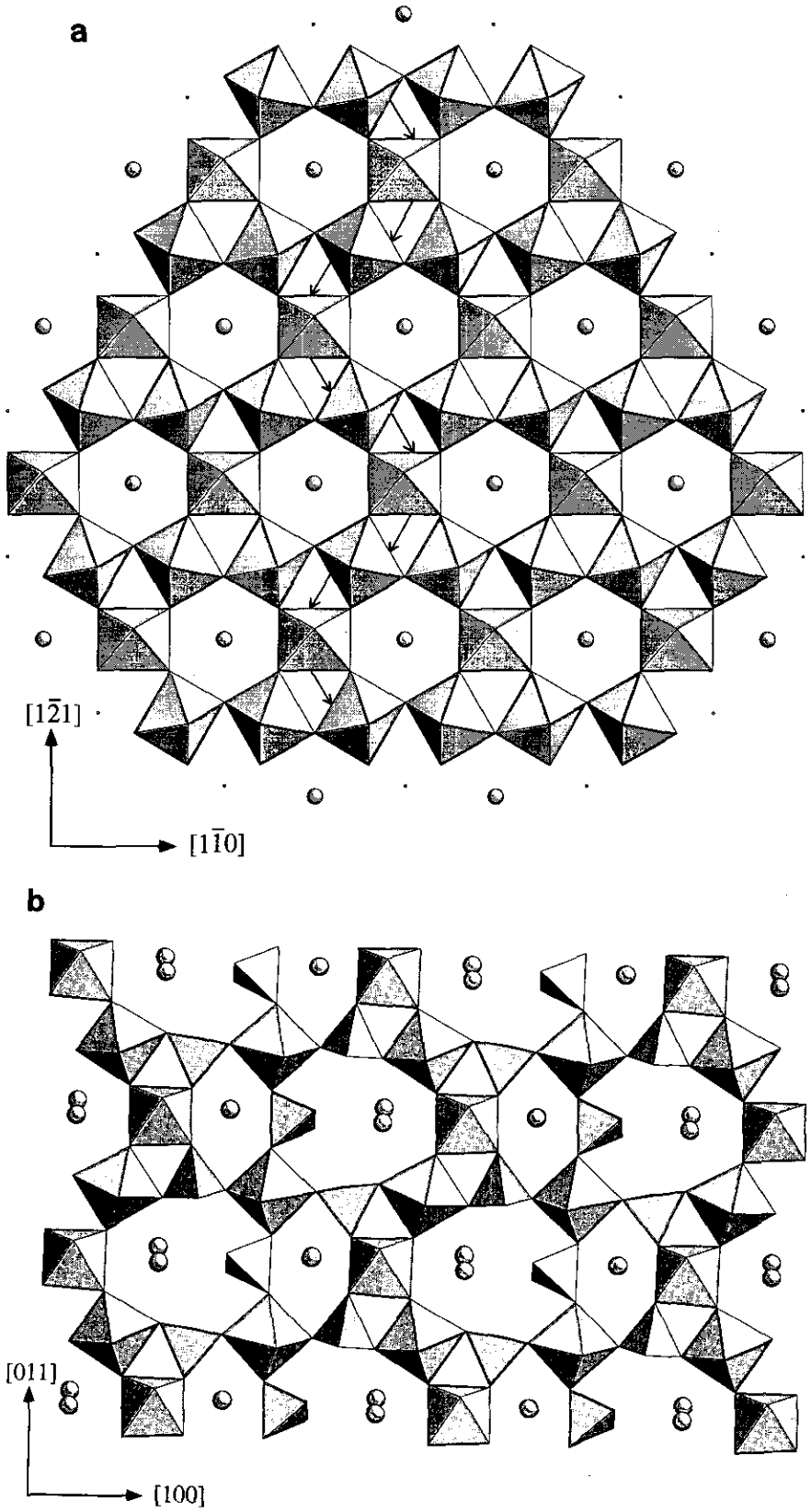

FIG. 4. Comparison of (a) cubic CTA/CTP structure with (b) orthorhombic KTP-type structure. The "octahedra" in (a) represent a disorder of octahedra and tetrahedra. The orthorhombic structure (b) is related to the cubic structure (a) by a simple tetrahedra–octahedra ordering. The characteristic *cis–trans–cis* chains of (b) can also be found in (a) (arrows).

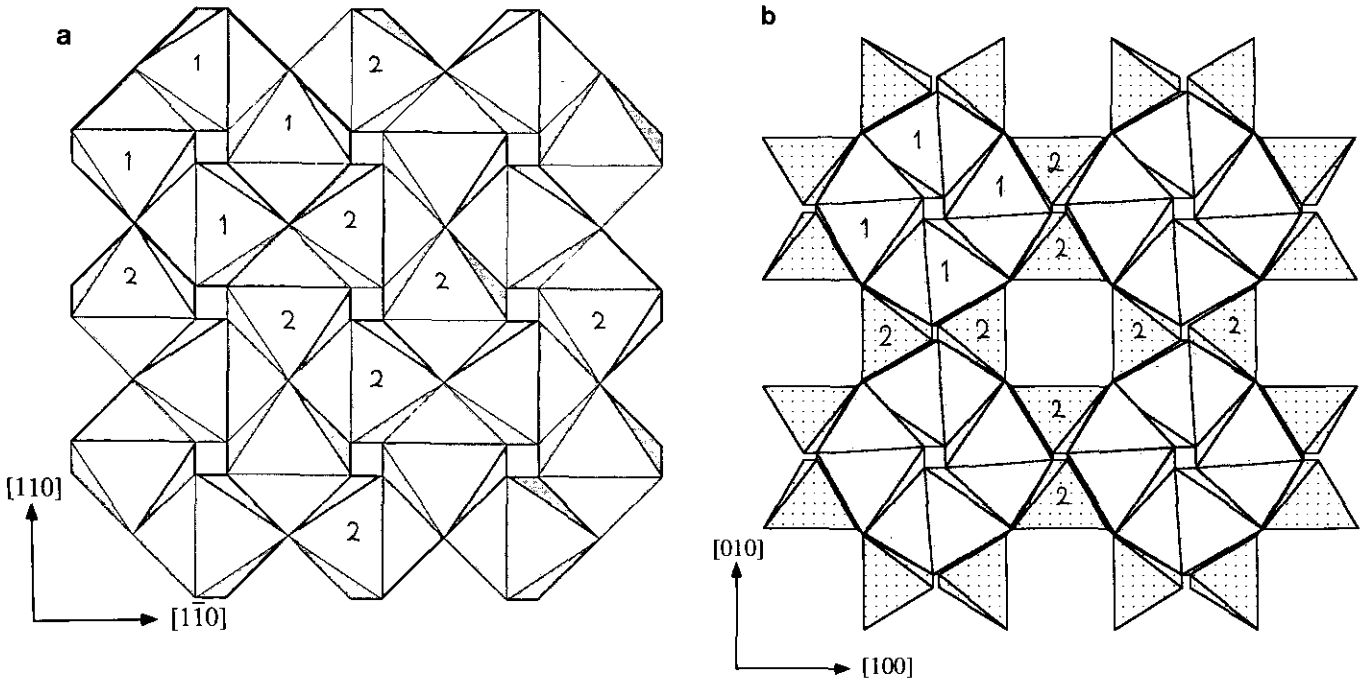

FIG. 5. Comparison of (a) cubic CTA/CTP with (b) $K(Mg_{1/3}Nb_{2/3})OPO_4$ (KMNP). "Octahedra" in (a) represent a disorder of octahedra and tetrahedra. The tetragonal structure (b) is again an ordered version of the cubic parent structure (a). The "octahedra" labeled 2 in (a) represent the tetrahedra in (b).

axis, Fig. 5. In this case, the tetragonal cell can be transformed into the cubic CTA/CTP cell as $a_{KMNP} \rightarrow 1/2[110]_{cub}$, $c_{KMNP} \rightarrow [001]_{cub}$.

Another structure type consisting of *cis–cis* linked Ti-chains is found in γ-$NaTiOPO_4$ (γ-NTP) (21). Based on the figure shown in the original publication (22) this structure again appears to be an ordered derivative of cubic CTA/CTP. Unfortunately the geometry reported in (22) cannot be reconstructed from the unit cell, spacegroup, and coordinates given therein. Nevertheless it can be deduced from the picutre shown in (22) that the cubic cell is transformed directly into an orthorhombic cell by a distortion of the cubic parent cell.

In contrast to KTP, KMNP, and γ-NTP, the structural relationship between CTP/CTA and sphene ($CaTiOSiO_4$) cannot be deduced in terms of pure octahedra–tetrahedra ordering in the cubic structure. Although kinked *trans–trans* octahedral chains characteristic for sphene are easily found in cubic CTA/CTP, Fig. 4a, the structural topology is different. Whereas in sphene, each orthophosphate group links three Ti-chains, the *trans–trans* chains in cubic CTA/CTP are arranged such that any ordering scheme must result in only two *trans–trans* chains connected by a orthoarsenate/phosphate group. It can be speculated that this different polyhedral network topology is one of the reasons why in KTP, KMNP, and γ-NTP, neighboring chains have approximately parallel Ti-displacement vectors, whereas in sphene the orientation of off-center Ti atoms in neighboring chains is antiparallel, resulting in a centrosymmetric structure and therefore inhibiting any nonlinear optic and ferroelectric effects.

As recently shown by X-ray topography (23), the orthorhombic KTP phase frequently contains inversion twin lamellae parallel to $(100)_{orth}$ and $(011)_{orth}$. Since $(100)_{orth}$ transforms into a mirror-plane in the cubic phase ($\{110\}_{cub}$), orthorhombic twinning along $(100)_{orth}$ becomes indistinguishable from regular lattice planes in the cubic phase. Twinning along $(011)_{orth}$, however, transforms into cubic $\{111\}$-twinning, which is consistent with the observation of the satellite reflections at $(h, k, l)n/3$ ($n = 1, 2$). Topologically, this twinning is caused by the insertion of true HTB-stacking into the stacking of the cubic CTA/CTP structure. Thus the strong twinning in the cubic phase, which makes it impossible to solve the structure from single-crystal data, is related to the twins and domains of the orthorhombic phase.

The simple relationship between orthorhombic and cubic CTA suggests that the phase transition occurs through dynamic exchange between Ti and As on the cation sites. This implies that at the phase transition the cations are very mobile and exchange randomly while the oxygen framework undergoes only minor changes. The phase transition reduces the two different, highly stressed Cs-positions in the orthorhombic phase to one single site in the cubic structure. The differences in coordination stress for the Cs cation can be quantified with the bond-valence

model (24). In this approach, the strength of each bond can be determined from two basic assumptions, (i) that the sum of all bond valences incident at any given atom in the structure (bond-valence sum) must equal the respective atomic valence and (ii) that the sum of the bond valences around any closed loop in the structure must be zero. The bond valences calculated from these rules correlate with observed bond lengths such that for any given cation–anion pair bond lengths and bond valences are directly transferable into each other. This therefore allows us to compare actual "observed" bond valences (derived from observed bond lengths) with their ideal values as calculated from the topology using the above-mentioned rules in individual structures. In the absence of any electronic effects and systematic errors in the structural data, deviations of the observed bond valences from their ideal value reflect steric strain within the structure. In particular, it is the bond-valence sum which can be used to reveal any steric stress in the structural arrangement, for example, a compressed structural unit will exhibit bond-valence sums which are too high, whereas an atom subject to tensional stress will show negative deviations of the bond-valence sum from the atomic valence. A rough bond-valence sum estimated by weighting each Cs–O bond by the occupancy of the respective oxygen site of the disordered model and noting that the deviation of the Cs bond valence sum from 1 is an indication of its coordination stress, clearly shows that the Cs coordination in the cubic phase is much less stressed (bond-valence sum = 0.96 v.u.) than in the orthorhombic phase (average bond-valence sum = 1.87 v.u.). Cheng *et al.* (4) hypothesized that the phase transition from the orthorhombic to the cubic CTA-structure might be triggered by this mismatch between the ideal size of the Cs^+-ion and the available space in the orthorhombic structure ("threatened structure model"). To extend the predictive possibilities of this model, an attempt was made to place the threatened structure model onto a more quantitative basis using again the bond-valence model. In order to also compare the bond-valence sums of alkali cations in hypothetical KTP-type compounds (e.g., orthorhombic CTP) on a common basis, the sums were all calculated using the fractional coordinates of KTP (25) for titanyl-phosphates and KTA (26) for titanyl-arsenates and cell parameters obtained from the following functions:

$$a = 1.706 \cdot \mathrm{IR(alkali\text{-}cation)} + 2.610 \cdot \mathrm{IR(octahedral\ site)} + 1.640 \cdot \mathrm{IR(tetrahedral\ site)} + 8.274.$$

$$b = 1.282 \cdot \mathrm{IR(alkali\text{-}cation)} + 0.980 \cdot \mathrm{IR(octahedral\ site)} + 1.077 \cdot \mathrm{IR(tetrahedral\ site)} + 3.594.$$

$$c = 4.254 \cdot \mathrm{IR(octahedral\ site)} + 0.994 \cdot \mathrm{IR(tetrahedral\ site)} + 7.834.$$

TABLE 5

Bond Valence Deviation of Alkali Cation and Orthorhombic-to-Cubic Phase Transition Temperatures for Various KTP-Type Compounds

Compound	Δbvs[a] (v.u.)	IR(^{IX}alk.cat.) (Å)	T_T[b] (°C)
$KTiOAsO_4$	0.09	1.55	*mm*2 stable
$TlTiOAsO_4$	0.19	1.60	*mm*2 stable
$KTiOPO_4$	0.21	1.55	*mm*2 stable
$TlTiOPO_4$	0.31	1.60	1048
$RbTiOAsO_4$	0.43	1.63	*mm*2 stable
$RbTiOPO_4$	0.59	1.63	1101
$CsTiOAsO_4$	0.90	1.78	963
$CsTiOPO_4$[c]	1.11	1.78	No *mm*2

[a] Δbvs, average bond-valence sum of alkali cations minus 1.
[b] Temperature of orthorhombic-to-cubic phase transition. Transition temperatures as given in (1).
[c] Orthorhombic structure hypothetical.

These functions were obtained from a least-square fit to a plot of observed cell parameters versus ionic radii (27) of cations of the first seven compounds listed in Table 5.

Bond-valence sums for the alkali cations obtained by this procedure are therefore automatically corrected for inherent differences of the framework size due to different framework–cation and alkali–cation sizes. Deviations of the calculated bond valences from their ideal values are given in Table 5, together with the corresponding transition temperature if applicable. Despite the small size of the data set, it is apparent that the transition temperature correlates inversely with the bond-valence deviation, except for $TlTiOPO_5$ (TTP), which seems to lie outside the general trend. This can however be explained by a lone pair effect characteristic of Tl^+ which causes additional electronic effects not allowed for in the bond-valance approach (28). Disregarding the TTP outlier, one may predict that any KTP-type structure with an average bond-valance deviation (Δbvs = observed bond-valance sum minus atomic valence) of 0.90 v.u. or less for the alkali cations has a finite stability field for the orthorhombic phase. On the other hand, it can be seen that the threshold for the cubic-phase field in terms of the bond-valence misfit is somewhere between 0.43 and 0.59 v.u.

In addition to the equilibration of the two Cs-sites, Ti^{4+} and As^{5+} start to disorder until they are randomly distributed over a single set of sites. In order to satisfy crystal chemical requirements, the disorder between Ti^{4+} and As^{5+} must be accompanied by rearrangement of the oxygens around As^{5+}. Although this effect is assumed to occur dynamically near the phase transition, it is not expected to be still dynamic at lower temperatures but rather to be in the form of a frozen-in static disorder.

A final striking result of this study is the apparent disagreement between the present chemical composition as

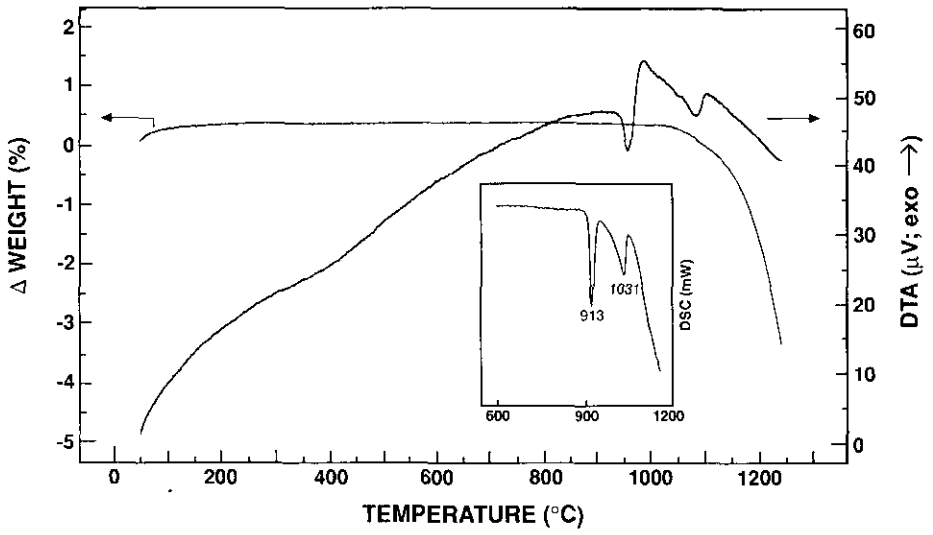

FIG. 6. Combined TGA/DTA (DSC inset). Only the second DTA event is accompanied with a weight loss in the TGA curve. This is in accordance with the observed stoichiometric phase transition before melting.

determined from both microprobe data and refinement results, and the report of a Cs deficiency in cubic CTA in (4) as deduced from ICP experiments. Thus, we undertook a careful reexamination of the orthorhombic-to-cubic phase transition using both DTA/TGA and DSC. As can be seen in Fig. 6, the DTA/TGA experiment showed an endothermic event with no associated weight loss at 935°C, correlating with the orthorhombic-to-cubic phase transition. Thus the lack of any loss of Cs is consistent with the present finding of a stoichiometric content. A second endotherm which is accompanied by weight loss occurs at 1050°C, interpreted as incongruent melting of the cubic phase (4). However, since it is not known whether the early stages of the weight loss are associated with cesium loss while the structure is still cubic, we cannot at present rule out the possibility of some degree of nonstoichiometry in cubic CTA. Moreover, we have some preliminary evidence (based on unit cell volume and reaction chemistry observations) that strongly suggests the cubic phase is in fact not a line phase and has an appreciable degree of nonstoichiometry. This observation and the difficulties of obtaining an accurate determination of Cs-content in these crystals using ICP most likely account for the apparent compositional inconsistencies between the present and previous results. Work is in progress to resolve these issues.

ACKNOWLEDGMENTS

We thank Dr. Yanbin Wang for the TEM diffraction pictures. This work was supported by the DuPont Company and by the NSF through Grant DMR 90242249 to J.B.P. The SUNY X3 beamline is supported by the Department of Energy through Grant DEFG-0286-ER-45231. M.G. wishes to acknowledge the support of the NSF-sponsored 1993 Summer Research Program in Solid State Chemistry for Undergraduates and Faculty. The National Synchrotron Light Source, Brookhaven National Laboratory, is supported by the U.S. Department of Energy, Division of Materials Sciences and Division of Chemical Sciences. The neutron experiment was conducted at the High Flux Beam Reactor, Brookhaven National Laboratory, and supported by the Division of Materials Sciences, U.S. Department of Energy, under Contract No. DE-AC02-76CH00016.

REFERENCES

1. J. Protas, G. Marnier, B. Boulanger, and B. Menaert, *Acta Crystallogr.* **C45,** 1123 (1989).
2. I. Tordjman, R. Masse, and J. C. Guitel, *Z. Kristallogr.* **139,** 103 (1974).
3. L. K. Cheng, L. T. Cheng, F. C. Zumsteg, J. D. Bierlein, and J. Galperin, *J. Cryst. Growth* **132,** 289 (1993).
4. L. K. Cheng, E. M. McCarronIII, J. Calabrese, J. D. Bierlein, and A. A. Ballman, *J. Cryst. Growth* **132,** 280 (1993).
5. A. G. Airapetyan, G. S. Damazyan, A. L. Manukyan, and A. S. Vagansaryan, *Russian J. Inorg. Chem.* **32,** 1068 (1987).
6. J. A. Kaduk, J. Faber, and S. Pei, *in* "American Crystallographic Association, Atlanta, 1994," Vol. 22, p. 141.
7. J. L. Pouchou and F. Pichoir, "Microbeam Analysis-1985." San Francisco Press, 1985.
8. M. B. Boisen and G. V. Gibbs, "Mathematical Crystallography." Mineralogical Society of America, 1985.
9. L. Passell, S. Bar-Ziv, D. W. Gardner, D. E. Cox, and J. D. Axe, *Mater. Sci. Forum* **79–82,** 475 (1991).
10. J. D. Axe, S. Cheung, D. E. Cox, L. Passell, T. Vogt, and S. Bar-Ziv, *J. Neutron Res.* **2,** 85 (1994).
11. T. Vogt, L. Passell, S. Cheung, and J. D. Axe, *Nucl. Instrum. Methods* **A338,** 71 (1994).
12. A. LeBail, *in* "Accuracy in Powder Diffraction II" (E. Prince and J. K. Stalick, Eds.) Special Publ. 846, pp. 213. National Institute of Standards and Technology, Gaithersburg, MD, (1992).
13. C. J. Howard, *J. Appl. Crystallogr.* **15,** 615 (1982).
14. P. Thompson, D. E. Cox, and J. B. Hastings, *J. Applied Crystallogr.* **20,** 79 (1987).
15. A. C. Larson and R. B. VonDreele, "GSAS, Los Alamos Report LAUR 86-748." 1986.

16. A. Altomare, G. Cascarano, C. Giacovazzo, and A. Guagliardi, "SIRPOW.92—A Direct Method Package for Structure Solution from Powder Data." 1992.
17. W. C. Hamilton, *Acta Crystallogr.* **18,** 502 (1965).
18. A. Magneli, *Acta Chem. Scand.* **7,** 315 (1953).
19. A. Leclaire, M. M. Borel, A. Grandin, and B. Raveau, *J. Solid State Chem.* **110,** 256 (1994).
20. E. M. McCarronIII, J. C. Calabrese, T. E. Gier, L. K. Cheng, C. M. Foris, and J. D. Bierlein, *J. Solid State Chem.* **102,** 354 (1993).
21. M. L. F. Philips, W. T. A. Harrison, G. D. Stucky, E. M. McCarronIII, J. C. Calabrese, and T. E. Gier, *Chem. Mater.* **4,** 222 (1992).
22. P. G. Nagornyi, A. A. Kapshuk, N. V. Stus', and N. S. Slobodyanik, *Kristallografyia* **35,** 634 (1990).
23. S. Wang, M. Dudley, L. K. Cheng, and J. D. Bierlein, *Mater. Res. Soc. Symp.* **307,** 243 (1993).
24. I. D. Brown, *Acta Crystallogr.* **B48,** 553 (1992).
25. P. A. Thomas, A. M. Glazer, and B. E. Watts, *Acta Crystallogr.* ***B46,*** 333 (1990).
26. M. ElBrahimi and J. Durand, *Rev. Chim. Mineral.* **23,** 146 (1986).
27. R. D. Shannon, *Acta Crystallogr.* **A32,** 751 (1976).
28. M. Kunz and I. D. Brown, *J. Solid State Chem.* **115,** 395 (1995).